A Low-Cost, High-Efficiency and Full-Metal Reflectarray Antenna with Mechanically 2-D Beam-Steerable Capabilities for 5G Applications

Mei, Peng; Zhang, Shuai; Pedersen, Gert Frølund

Published in:
I E E E Transactions on Antennas and Propagation

DOI (link to publication from Publisher):
10.1109/TAP.2020.2993077

Publication date:
2020

Document Version
Accepted author manuscript, peer reviewed version

A Low-Cost, High-Efficiency and Full-Metal Reflectarray Antenna with Mechanically 2-D Beam-Steerable Capabilities for 5G Applications

Peng Mei, *Student Member, IEEE*, Shuai Zhang, *Senior Member, IEEE*, and Gert Frølund Pedersen, *Member, IEEE*

***Abstract*—This paper presents a low-cost, high-efficiency and full-metal reflectarray (RA) antenna with mechanical beam-steerable capabilities. A unit cell (UC) implemented by a metal cylinder with a cuboid-shaped notch is proposed to achieve a 1-bit reflection phase (0 and π) for the transverse electric (TE) and transverse magnetic (TM) normal incidence waves. The proposed UCs can be employed to construct a RA antenna with 2-D beam-steerable abilities. For demonstration, the RA antennas with six different beam directions are presented as examples, by simply adjusting the rotations of the UCs. The impedance matches of the RA antenna are all below -10 dB from 22 to 33 GHz, and the measured radiation patterns of the RA antenna are all highly consistent with the simulated counterparts for the six different beam direction scenarios. A 1.5 dB gain drop bandwidth of approximately 20 % from 24.7 to 30 GHz and a peak realized gain of 18.9 dBi at 26 GHz are experimentally obtained for the RA antenna with radiation patterns at broadside. Compared to the substrate-based UCs loaded with PIN diodes, the proposed UCs have full-metal structures without using any active RF components and dielectric substrates, leading to the high total efficiency of the proposed RA antenna. Due to the low-cost, high-efficiency, and high-power handling properties, the proposed RA antenna can provide a fixed or scanning beam and is a good candidate for 5G millimeter-wave communication applications.**

***Index Terms*— RA antenna, full-metal structure, high-efficiency, low-cost, 2-D beam-steerable, 5G applications.**

I. Introduction

Antennas with beam-steerable capabilities have attracted lots of attention and interests since they can achieve versatile radiation performance. The classical and representative antennas to achieve beam-steerable capacities are phased arrays that every antenna element connects to a phase shifter [1]-[6]. By manipulating the phase shifting of every phase shifter, the phased array is able to realize a 2-D scanning beam. Since phase shifters are either bulky or lossy, the phased arrays are not good solutions for lightweight, high-flexibility and high-efficiency applications. The beamforming network is another effective technique to achieve 2-D scanning beams for a planar array [7]-[13]. However, the beamforming network would be very complicated and extremely lossy for large-scale arrays [10]-[13].

Recently, H. Kamoda *et al*., [14] proposed a 60-GHz electronically reconfigurable large reflectarray antenna to achieve steerable beams, where the authors designed a unit cell (UC) loaded with a PIN diode. By controlling the forward and reverse voltages of the PIN diode, the UC can provide two reflection phases with a 180 deg phase difference (e.g., 0 and π). Some approximations are made to replace the actual phase of every unit pixel (that usually ranges from - π to π) of a RA antenna with the 1-bit reflection phase provided by the UC. The measured results validated the effectiveness of their design. Afterward, many investigations based on the UC loaded with RF active components were widely carried out [15]-[20]. It should be noted that the usages of many PIN diodes would introduce extra losses to significantly decrease the total efficiencies of such antennas. And the reliability of applying so many PIN diodes simultaneously at millimeter-wave is also a severe issue that constrains the practical applications of such reconfigurable RA antennas. To avoid using PIN diodes, some other techniques were proposed to achieve steerable beams by mechanically rotating the substrate-based UCs as reported in [21]-[23], which can efficiently alleviate the losses caused by PIN diodes to increase the entire efficiency at some extent. In [24], the authors achieved a beam-scanning Fabry-Perot antenna at 11 GHz by mechanically rotating the metasurfaces with phase compensation performance located in the near field, which suffers from a narrow bandwidth and limited beam numbers once the configurations of the metasurfaces were fixed. It is worthwhile to point out, here, even though it has been widely acknowledged, that the losses and prices of active RF components and substrates would all significantly increase with the increment of the operating frequencies.

On the other hand, 5G millimeter-wave bands will be widely used in the near future due to the large available spectrum resources [25], [26]. Millimeter-wave antennas with 2-D beam-steerable capabilities with low-cost and high-efficiency are highly demanded in millimeter-wave communications. In this paper, a low-cost, high-efficiency, and full-metal RA

Manuscript received Nov, 2019. This work was supported in part by AAU Young Talent Program and also in part by the InnovationsFonden project of MARS2. (*Corresponding author: Shuai Zhang*)

The authors are all with the Antennas, Propagation and Millimeter-wave Systems (APMS) section, Department of Electronic Systems, Aalborg University, Aalborg, 9220, Denmark. (email: sz@es.aau.dk)

antenna with 2D beam-steerable capacities is proposed for 5G millimeter-wave applications, avoiding usages of any active RF components and dielectric substrates. A UC implemented by a metal cylinder with a cuboid-shaped notch is proposed to construct the proposed RA antenna. It is found that the proposed UC can provide a 1-bit reflection phase (0 and π) for the TE and TM normal incidence waves. Inspired by previously-reported reconfigurable RA antennas implemented by UCs loaded with PIN diodes [14]-[20], a RA antenna with 2-D beam-steerable capabilities can be readily achieved with the proposed UCs by controlling the reflection phases of the UCs. For demonstration, A RA antenna capable of six different main beam directions (e.g. broadside direction, 30 deg and 60 deg off-broadside in E-plane, 30 deg and 60 deg off-broadside in H-plane, and $\theta = 45$ deg, $\phi = 45$ deg) are presented by adjusting the rotation of every UC. Since the proposed UCs are composed of full-metal structures, it is sufficiently predicted that the total efficiency defined by "realized gain/directivity" of the proposed RA antenna would be very high. The simulated total efficiencies of the RA antenna with six different main beam directions are all over 95 %. In addition, it is found that the proposed RA antenna is dual-polarized and has potential abilities for circular polarization applications from the analysis.

The rest of the paper is organized as follows: Section II presents and describes the proposed UC with a full-metal structure, its reflection phases are investigated in detail. Section III introduces the implementations of the RA antenna with six different main beam directions by using the proposed UCs. Fabrications, measurements, and discussions are carried out in Section IV. Finally, some remarkable conclusions are drawn in Section V.

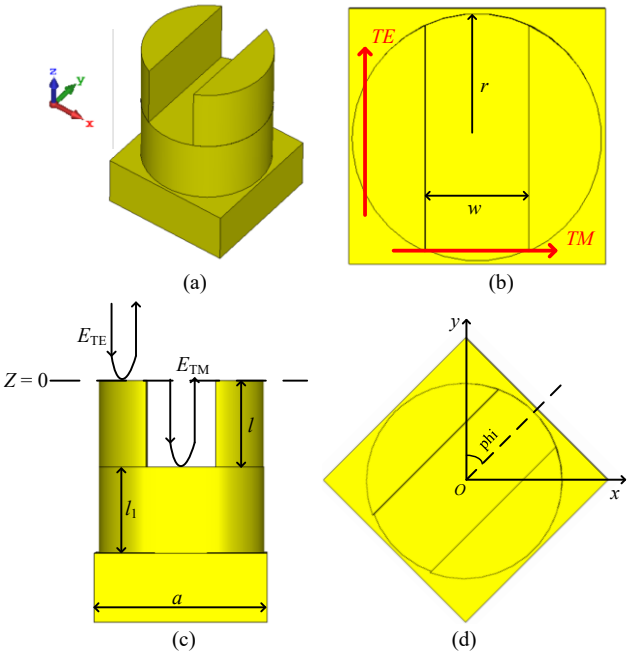

Fig.1. Geometries of the proposed UC with a 1-bit reflection phase property. (a). Perspective view. (b). Top view. (c). Side view. (d). Top view with a phi angle offset. (a=5mm, l_1=2.5mm, l=2.5mm. r=2.45mm, w=2mm.)

II. Unit Cell Design and Analysis

Fig.1 shows the geometries of the proposed UC with a full-metal structure. It consists of two parts: a square base, and a metal cylinder with a cuboid-shaped notch which is characterized by a width of w and a length of l. It should be noted that the proposed UC can produce different frequency responses for different polarizations of incidence waves. Specifically speaking, the proposed UC with a configuration shown in Fig. 1(b) is a polarization-invariant structure for the x- and y-polarized incidence waves, which means the reflected waves are still x- and y-polarized (polarization conversion efficiency is 0), respectively. However, when the proposed UC rotates a phi angle with z-axis as shown in Fig. 1 (d), it would demonstrate polarization rotation abilities with different polarization conversion efficiencies. Particularly, when phi = 45 deg, the proposed UC provides a perfect polarization rotation performance at a certain frequency (polarization conversion efficiency is 1). That is to say, the reflected wave is y-polarized for x-polarized incidence wave or vice versa. Here, we mainly serve the proposed UC as a polarization-invariant structure. For brevity, we specify that the TE wave is y-polarized while the TM wave is x-polarized. For a TE or TM wave impinging on the UC under normal incidences, the incident electric fields can be written as follows:

$$\overrightarrow{E_{i\,TE}} = \vec{y}E_0 e^{jkz}, \quad z \geq 0 \tag{1-a}$$

$$\overrightarrow{E_{i\,TM}} = \vec{x}E_0 e^{jkz}, \quad z \geq 0 \tag{1-b}$$

where k is the wavenumber in free space, E_0 is the amplitude of the electric field of incidence wave.

When electromagnetic waves arrive at the plane of z = 0 [as marked in Fig. 1(c)], some reflections and transmissions for TE and TM incidence waves happen. However, it is found that electromagnetic reflections are dominated for TE incidence wave at the plane of z = 0, while electromagnetic transmissions are dominated for TM incidence wave on the same plane. The transmitted TM wave would propagate along the cuboid-shaped notch and be reflected at the plane of z = -l, and then propagate along the cuboid-shaped notch again. Therefore, the reflected electric fields for TE and TM normal incidence waves are approximately formulated as follows:

$$\overrightarrow{E_{r\,TE}} \approx \vec{y}\Gamma_1 e^{j\varphi_1} \cdot E_0 e^{-jkz}, \quad z \geq 0 \tag{2-a}$$

$$\overrightarrow{E_{r\,TM}} \approx \vec{x}\Gamma_2 e^{j\varphi_2} \mathrm{T}^2 e^{j2\phi} E_0 e^{-j(kz-2kl)}, \quad z \geq 0 \tag{2-b}$$

where Γ_1 and φ_1 are reflection amplitude and phase at the plane of z = 0 of TE normal incidence wave, respectively. T and ϕ are transmission amplitude and phase at the plane of z = 0 of TM normal incidence wave, respectively. Γ_2 and φ_2 are reflection amplitude and phase at the plane of z = -l of TM normal incidence wave, respectively. For the proposed UC, it is acknowledged that Γ_i and φ_i (i=1,2) are all approaching to 1 and π, respectively. Therefore, we can regard $\Gamma_1 \approx \Gamma_2$ and $\varphi_1 \approx \varphi_2$ approximately.

Based on the reflected electric fields, the phase difference of TE and TM normal incidence waves at the plane of z = 0 is calculated and obtained as follows:

$$\Delta\varphi = 2kl + 2\phi \tag{3}$$

If $\Delta\varphi$ is equal to π, Eq. (3) yields to:

$$l = (\frac{1}{4} - \frac{\phi}{2\pi})\lambda \tag{4}$$

It should be noted that the transmission phase ϕ is sensitive to the operating frequency f and width of the cuboid-shaped notch w, which is difficult to obtain its exact value. However, based on the Eq. (4), the value of l can be initially given to λ/4. Then, the desired phase difference (e.g. π) can be obtained by tuning l slightly.

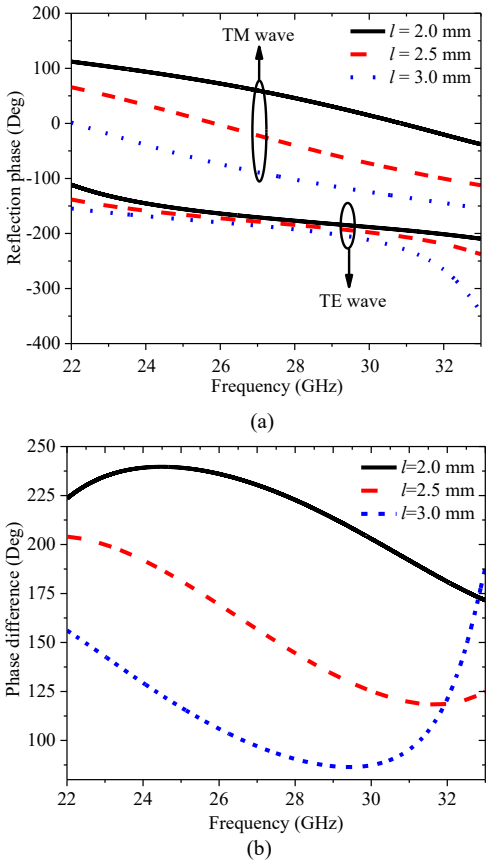

Fig.2. The reflection phase properties of the proposed UC under TE and TM normal incident waves. (a). The reflection phase under TE and TM wave with different values of l. (b). The phase difference with different values of l. (a=5mm, l_1=2.5mm, r=2.45mm, w=2mm.)

According to the analysis above, some simulations are carried out with CST Microwave Studio to check the performance of the proposed UC, where the periodic boundary conditions (PBCs) are imposed on the UC to simulate an infinite surface to obtain the desired results. The reflection phases and phase differences of TM and TE normal incidence waves with different values of l and other parameters fixed are firstly simulated. As seen in Fig. 2 (a), the reflection phases of the proposed UC are more sensitive to the value of l for TM normal incidence wave, which can be explained from Eq. (2-b). From Fig. 2(b), the frequency with a phase difference equal to π is shifting toward a higher frequency with the decrement of l as can be deduced from Eq. (3). When l = 2.5 mm, a 180 deg phase difference is obtained at the frequency of 25 GHz. Note that, the quarter-wavelength at 25 GHz is 3.0 mm that is bigger than 2.5 mm. The result is highly consistent with Eq. (4) that the transmission phase ϕ has effects on the value of l.

From the simulated results, it is concluded that the proposed UC can provide two-phase states with a 180 deg phase difference for a proper value of l. Therefore, a 1-bit digital code is used to characterize the reflection phase of the proposed UC as listed in Tab. I.

Tab. I. Reflection phase characterization with a 1-bit digital code for the proposed UC

State	Code	Phase
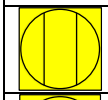	"0"	0
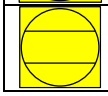	"1"	π

As stated and concluded before, the transmission phase ϕ would affect the final reflection phase for TM normal incidence wave, and ϕ is closely associated with the width of the cuboid-shaped notch w and operating frequency f. Tuning w could be an effective technique to control the bandwidth on the reflection phase difference. Here, simulations are carried out with different values of w to check the phase differences of TE and TM normal incidence waves. As seen in Fig. 3, the slope of the phase differences is becoming smoother with the increment of w. It is concluded that a wider bandwidth on phase difference can be achieved with a bigger value of w to some extent. Considering the mechanical milling precision and preventing the cuboid-shaped notch from deformation, the value of w is chosen as 2.0 mm.

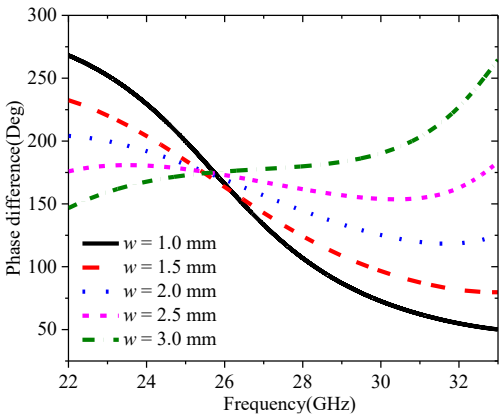

Fig.3. The phase difference of the UC under TE and TM normal incident waves with different values of w.

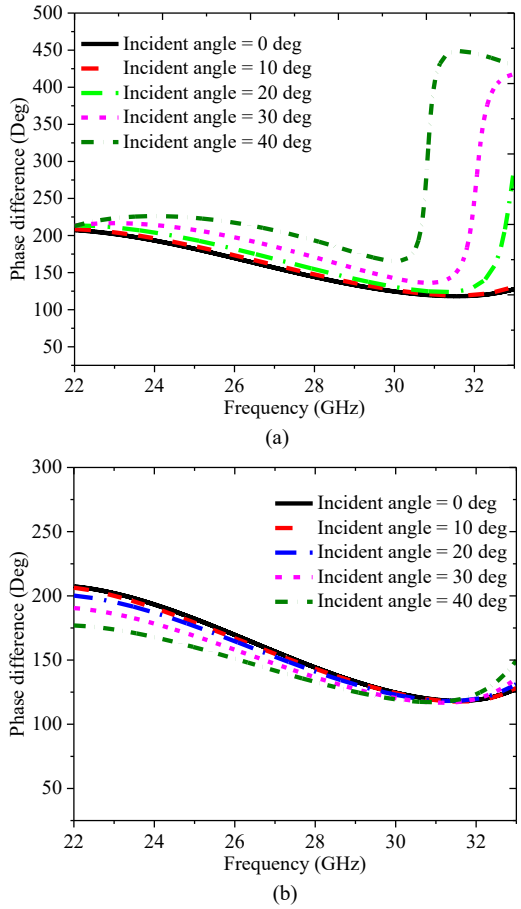

Fig.4. The reflection phase difference of the proposed UC under oblique incidences. (a). TE oblique incident wave (b). TM oblique incident wave.

The reflection phase difference of the proposed UC for TE and TM oblique incidence waves are also simulated and presented. Fig. 4 presents the phase differences of the state "0" and state "1", where it is observed that the phase differences are relatively stable for TE and TM oblique incidence waves until the oblique incidence angle reaches 40 deg from 22 to 30 GHz. The stable phase differences make the proposed UCs good candidates for a RA antenna design.

III. Implementation of the Proposed RA Antenna

In this section, the proposed UCs with a 1-bit reflection phase are fully employed to construct a RA antenna with mechanically 2-D beam-steerable capabilities. Fig. 5 presents a schematic diagram of a RA antenna. It consists of a feeding source and a reflective array with full reflectance and phase compensating properties. A linearly-polarized horn antenna with a model of "PASTERNACK PE9851/2F-10" operating from 22 to 33 GHz is adopted as the feeding source. The dimensions and radiation patterns of the feeding source are available from its datasheet [27]. The simple centrally-fed method is adopted here to verify the concept and effectiveness of the proposed RA antenna. An offset-fed method can be chosen to replace the centrally-fed one to lower its blockage effects on the gain of a RA antenna [28]-[30]. It is widely acknowledged that the phase distributions on the reflective array plane are closely associated with the distance of F and the frequency of interest, and the aperture efficiency of a RA antenna is typically determined by the size of reflective array D, distance F, and the radiation beam of the feeding source that is usually characterized with $\cos^q(\theta)$ [31]. In our design, a low profile and small size are desired, so we select the values of F and D 40 mm and 70 mm, respectively. The polarization of the linearly-polarized feeding source is y-polarized as depicted in Fig. 5. Once the dimensions of the proposed RA antenna are determined, the electric fields and phase distributions on the reflective array surface at 26 GHz can be obtained by simulations.

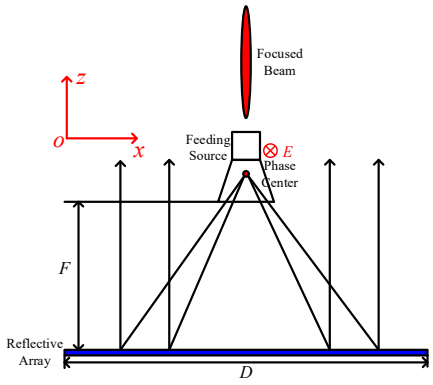

Fig. 5. Schematic diagram of a RA antenna.

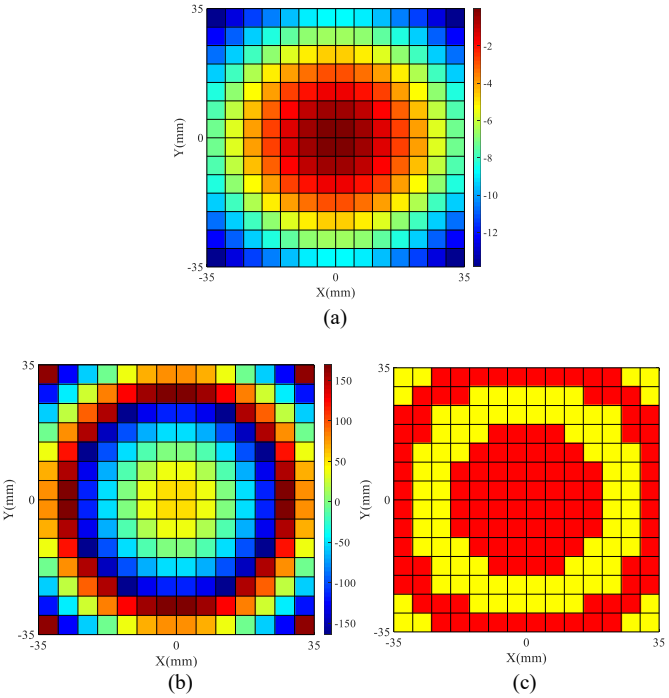

Fig. 6. The electric fields and phase distributions on the reflective array surface at 26 GHz. (a). Electric field distributions. (b). Desired phase distributions. (c). Actual phase distributions that the proposed UCs provide. (The red and yellow blocks represent π and 0, respectively.)

Fig. 6 plots the electric fields and phase distributions on the reflective array surface at 26 GHz for a broadside radiation

pattern. As seen in Fig. 6 (a), the electric fields reach peak values on the center of the reflective array surface, and the illumination taper of the electric field is about -9 dB at the edge of the reflective array surface. It is also clearly observed that the desired phase on every UC ranges from -180 to 180 degrees in Fig. 6 (b). However, the proposed UC can only provide a 1-bit reflection phase (e.g. 0 and π). Therefore, some approximations should be made to make the UCs suitable for the proposed RA antenna design:

$$\varphi_{actual} = \begin{cases} 0, & -\frac{\pi}{2} < \varphi_{desired} < \frac{\pi}{2} \\ \pi, & Otherwise \end{cases} \quad (5)$$

where φ_{desired} is the desired phase on every unit pixel obtained from the simulations, and φ_{actual} is the actual phase that the proposed UC can provide for the corresponding unit pixel. Using the above approximations, the phase distributions on the preselected reflective array plane are updated as shown in Fig. 6 (c). Based on the actual phase distributions, a RA antenna can be easily implemented by the proposed UCs with proper rotations.

If the main beam of a RA antenna is off-broadside, some phase gradients on the reflective array plane should be imposed. To determine the desired phase compensation on every UC to achieve a beam off-broadside, we can consider the reflective array as a planar array. Every UC in the reflective array can be equivalently regarded as a radiation element. Supposed that a radiation beam is pointing toward (θ_0, φ_0), the progressive phases of two adjacent UCs in x and y-direction can be calculated by:

$$\beta_x = -kd_x \sin\theta_0 \cos\varphi_0 \quad (6\text{-a})$$

$$\beta_y = -kd_y \sin\theta_0 \sin\varphi_0 \quad (6\text{-b})$$

where β_x and β_y are progressive phases in x- and y-direction, respectively. k is the wavenumber in free space, d_x and d_y are element space in x- and y-direction, respectively. Once the required main beam direction (θ_0, φ_0), the element space in x- and y-direction, and the interested frequency are all determined, the progressive phases are readily calculated by using Eq. (6).

Here, six different main beam directions at 26 GHz are demonstrated: a). broadside direction; b). 30 deg off-broadside in E-plane; c). 60 deg off-broadside in E-plane; d). 30 deg off-broadside in H-plane; e). 60 deg off-broadside in H-plane; f). θ = 45 deg and φ = 45 deg.

It should be noted that the additions of phase gradients should be added based on a uniform phase distribution. Specifically speaking, for the desired main beam of 30 deg off-broadside in E-plane, the desired phase distributions on the reflective array plane should be obtained by adding the progressive phase in x-direction calculated with Eq. (6-a) to the uniform phase distribution shown in Fig. 6 (a). Once the desired phase distributions for the main beam of 30 deg off-broadside in E-plane are obtained, the actual phase distributions are determined by using the approximations illustrated in Eq. (5). The final phase distributions on the reflective array plane with the main beam of 30 deg off-broadside in E-plane are presented in Fig. 7(a). The actual phase distributions for the remaining four cases are all obtained by using the same approach, as shown in Figs. 7(b)-(e).

Based on the actual phase distributions shown in Fig. 6 (c) and Fig. 7, it is interesting found that a 2-D beam-steerable capability can be achieved by simply adjusting the rotation of every UC of the RA antenna. In this paper, we adjust the rotation of every UC manually to validate the effectiveness of the proposed RA antenna with 2-D beam-steerable capabilities.

As the feeding source is linearly-polarized, the proposed RA antenna has the same polarization accordingly. It should be noted, however, that the proposed RA antenna would be dual-polarized when a dual-polarized feeding source is used and the beam directions for the two polarizations are the same since we adopt a proper phase quantization (0 and π) to implement the reflective array. Even though the proposed UCs don't have abilities to covert a linear polarization of feeding source to a circular polarization for the proposed RA antenna, a circularly-polarized RA antenna would be obtained when the feeding source is a circular polarization as reported in [21].

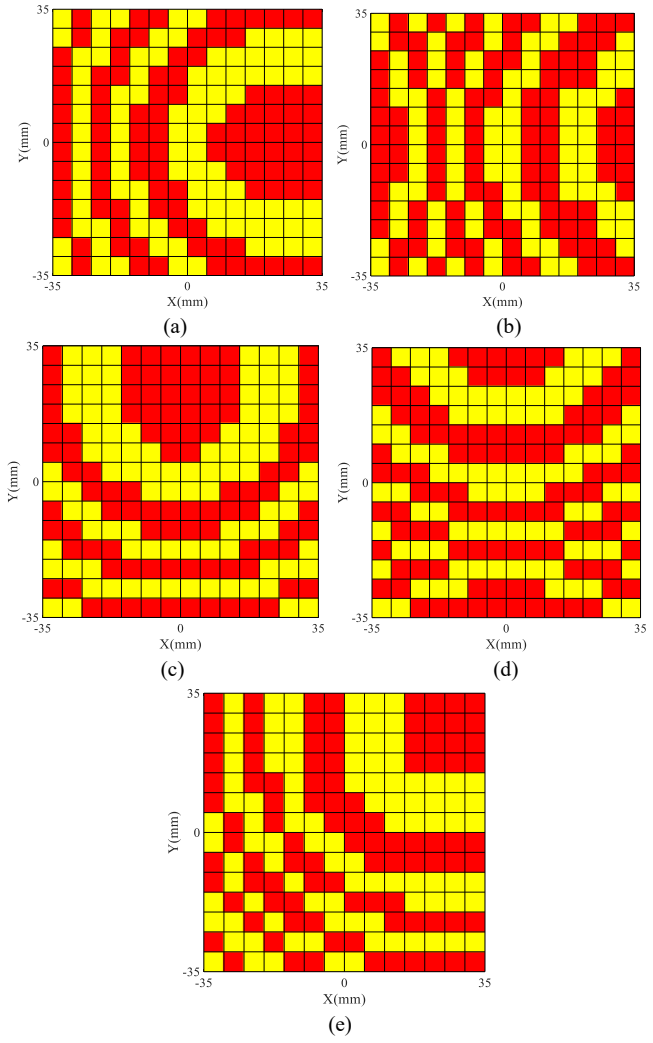

Fig. 7. The phase distributions on the reflective plate plane at 26 GHz. (a). 30 deg off-broadside in E-plane. (b). 60 deg off-broadside in E-plane. (c). 30 deg off-broadside in H-plane. (d). 60 deg off-broadside in H-plane. (e). φ = 45 deg and θ = 45 deg. (The red and yellow blocks represent π and 0, respectively.)

IV. Fabrication, Measurement, and Discussion

In this section, the proposed RA antenna is fabricated and its performance is evaluated experimentally. The base and UCs are all manufactured with material Aluminium by using mechanical milling technologies. The UCs are all tightly attached and fixed on the base with metallic screws, pads, and springs to avoid the air gap between the UCs and the base. A 3-D printed fixture is used to hold the feeding source and make the accurate separation from the feeding source to the reflective array. The assembled antenna prototype is shown in Fig. 8. Its reflection coefficients are measured with keysight Power Network Analyzer (PNA), radiation patterns and realized gains are evaluated with our advanced anechoic chamber.

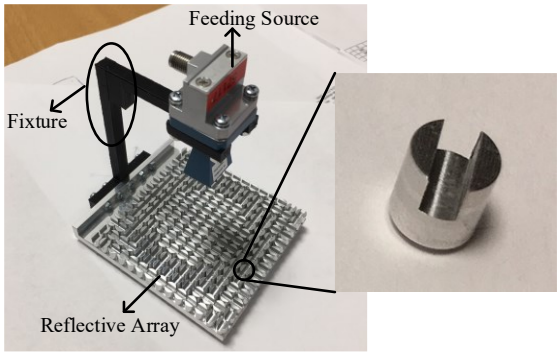

Fig.8. The photograph of the proposed RA antenna.

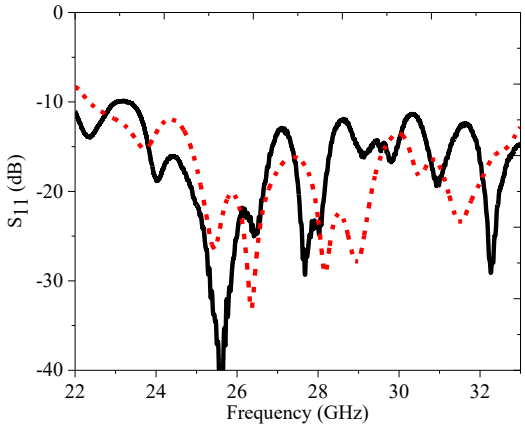

Fig. 9. Measured and simulated reflection coefficients of the proposed RA antenna at broadside direction.

A. Reflection coefficients.

Fig.9 presents the measured reflection coefficients of the proposed RA antenna with radiation pattern at broadside, where the simulated counterpart is also plotted for comparison. It is observed that the measured and simulated results agree well with each other, revealing that the reflection coefficients are all below -10 dB from 22 to 33 GHz. Since the blockage of the feeding source would impact the reflection coefficient of the proposed RA antenna with radiation patterns at broadside, it is sufficiently reasonable to predict that the measured reflection coefficients for the other five scenarios are all below -10dB from 22 to 33 GHz, which are all verified by the corresponding measured results that are not presented here.

B. Realized gain and radiation patterns

Fig. 10 gives the measurement environment and setup. The measurement setup can be used to measure 3-D radiation patterns of an antenna. The dual-polarized horn antenna at the top ceiling is served as a receiving antenna. The rotary arm connecting to the receiving antenna can rotate in the vertical plane (*yoz*-plane). The rotary table can rotate 360 deg in the horizontal plane (*xoy*-plane). It should be mainly pointed out that the rotation directions of the rotary table and arm correspond to $\boldsymbol{\phi}$ and $\boldsymbol{\theta}$, respectively, as marked in Fig. 10. The rotary arm can rotate clockwise continuously. The 0 deg means that the receiving antenna is located at the top ceiling or we can consider the receiving antenna is in the *z*-axis. The rotation resolution of the rotary arm and table can be controlled independently with a computer. Since the proposed RA antenna has six different radiation patterns to be measured, we set the rotation resolution of the rotary arm and table as 5 and 2 deg to save time and ensure the measurement accuracy at the same time. On the other hand, the radiation patterns of the proposed RA antenna are mainly concerned from -90 to 90 deg, the rotary arm, therefore, is set from 0 to 90 deg to further save measurement time with the rotary table from 0 to 360 deg in the horizontal plane (*xoy*-plane).

The realized gains of the proposed RA antenna with a radiation beam at broadside direction are measured from 24 to 30 GHz, where the simulated directivities and realized gains are also plotted for comparison. As seen in Fig.11, the measured realized gains are smaller than the simulated results, the discrepancies are mainly attributed to the following reason besides measurement and assembling tolerances: the effects of the coaxial to waveguide transition of the feeding source are not considered in simulations since its specific dimensions are not available from its datasheet. However, the measured realized gains include the losses of the coaxial to waveguide transition structure, leading to the lower measured realized gains compared with the simulated ones. The measured and simulated realized gains at 26 GHz are 19.5 dBi and 18.9 dBi with a gain difference of only 0.6 dB. From Fig. 11, it is observed that the maximal gain discrepancy between simulated and measured results is less than 1.0 dB from 24 to 30 GHz. Since the proposed RA antenna is a full-metal structure, only conductor losses (no substrate losses) are dominated, leading to the simulated realized gains very close to the simulated directivities as can be seen in Fig. 11. Here, the total efficiency defined by "realized gain/directivity" is proposed to evaluate the low losses property of the proposed RA antenna. Since the measured directivities are not available from the measurement setup, Fig. 11 plots the simulated total efficiencies with frequencies, where the total efficiency of more than 90 % is obtained from 24 to 30 GHz. Besides, it is observed from Fig. 11 that the measured 1.5

dB gain drop bandwidth of the proposed RA antenna reaches approximately 20 % from 24.7 to 30 GHz.

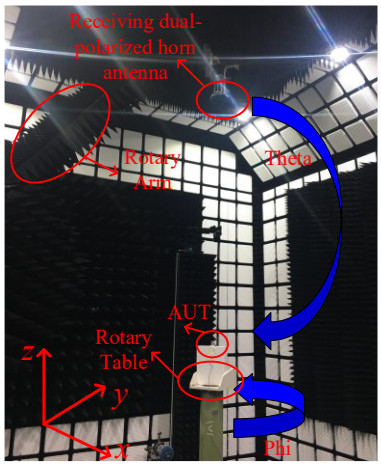

Fig. 10. Measurement setup.

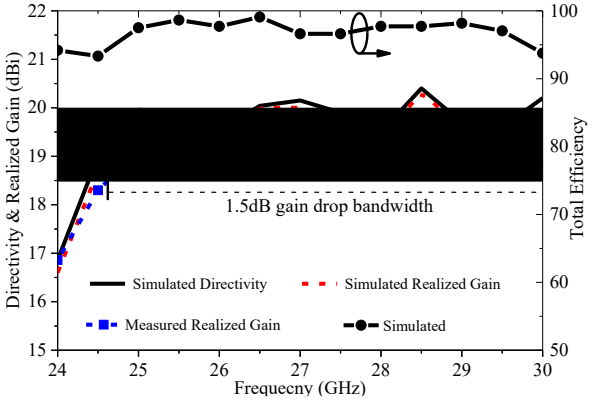

Fig. 11. Simulated directivity, realized gain, total efficiency, and measured realized gain of the proposed RA antenna with radiation beam at broadside.

To give more intuitive views on radiation patterns with the different main beam directions. The 3-D radiation patterns of the proposed RA antenna with six different main beam directions are measured and presented at 26 GHz. It should be noted that ϕ = 90 deg and ϕ = 180 deg in Fig. 12 correspond the E- and H-plane of the RA antenna, respectively according to the relative positions of the measurement setup. From Fig. 12 (a), it is observed that maximum gains are always concentrated at the location of θ = 0 deg and ϕ ranging from 0 to 360 deg, which means the main beam points to broadside direction. From Figs. 12 (b)-(f), it is clearly seen that the maximum gains are located at a certain position. Figs. 12 (b)-(c) present the 3-D beam-steerable radiation patterns in E-plane, it is observed that the measured maximum gain is pointing to 30 and 60 deg approximately, respectively. Likewise, as seen in Figs. 12 (d)-(e), the measured maximum gain is pointing to 30 and 60 deg in H-plane approximately, respectively. Fig. 12 (f) shows the measured 3-D radiation pattern whose beam points to θ = 45 deg and ϕ = 45 deg (135 deg). All the measured main beam directions are highly consistent with the prescribed and calculated main beam directions.

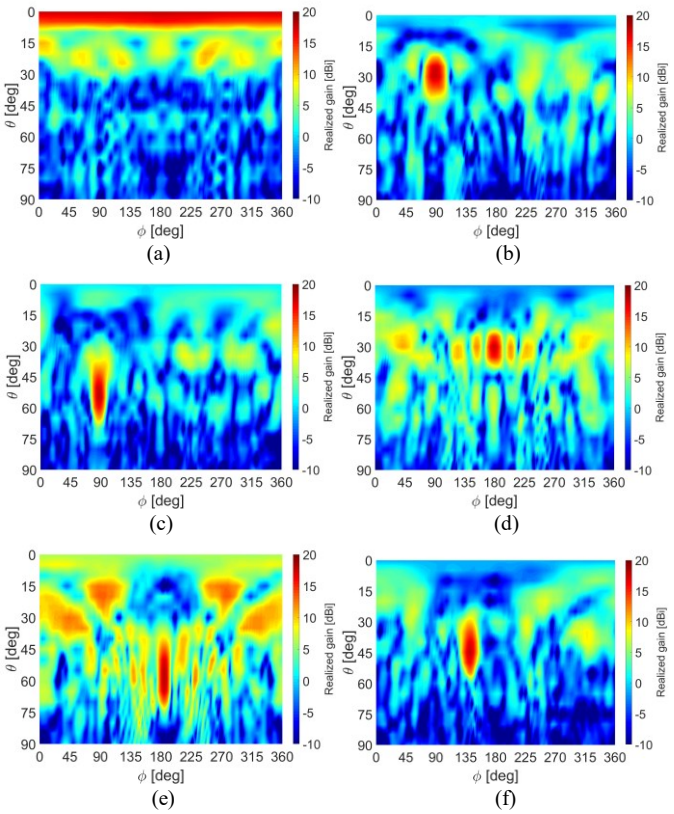

Fig.12. Measured 3-D realized gains of the proposed RA antenna with six different radiation beam directions at 26 GHz. (a). At broadside. (b). At 30 deg off-broadside in E-plane. (c). At 60 deg off-broadside in E-plane. (d). At 30 deg off-broadside in H-plane. (e). At 60 deg off-broadside in H-plane. (f). At theta = 45 deg and phi = 45 deg (135 deg).

The 2-D radiation patterns of the proposed RA antenna capable of six different main beam directions are also presented and compared. Figs. 13 (a)-(b) give the measured normalized radiation patterns of the RA antenna in E- and H-plane with the main beam at broadside at 26 GHz, where the simulated counterparts are also plotted for comparison. It is observed that the measured and simulated results are consistent. The main beams, first radiation nulls, and sidelobes are almost identical. To clearly reflect the beam focusing property of the proposed RA antenna, the simulated radiation patterns in E- and H-plane of the feeding source and a RA antenna whose reflective array surface is replaced by the same size metallic surface are also supplied in Figs. 13 (a) and (b) at the same frequency. It is seen that the proposed RA antenna (18.9 dBi) has a much higher gain compared to the feeding source (10.3 dBi). Due to the finite size of the metallic surface, there are some minor gain dips in radiation patterns of a RA antenna with a metallic surface as shown in Fig. 13 (a) and (b). Since the proposed RA antenna is implemented by UCs with only a 1-bit reflection phase, the phase quantization errors would increase the sidelobe of the RA antenna as comprehensively investigated in [32]. The sidelobes in E- and H-plane are -8 dB and -9 dB, respectively. Figs. 13 (c)-(f) present the normalized radiation patterns with the different main beam directions in E- and H-plane, respectively. Except for Fig. 13 (e) that the measured sidelobes are slightly

higher than that of simulated results, the measured and simulated results shown in Fig. 13 (c), (d), and (f) are highly consistent regarding the main beams, radiation nulls, and sidelobes. Fig. 12 (g) shows the normalized radiation pattern of the proposed RA antenna whose main beam points toward θ = 45 deg and ϕ = 45 deg, where it is observed that the measured and simulated results have extremely great agreements in terms of main beams, radiation nulls, and sidelobes. As seen in Fig. 13, the sidelobes of the proposed RA antenna with the different beam pointing directions are all below -10 dB. Besides, the measured cross-polarization (cro-pol) levels on interested cut planes are also plotted in Fig. 13, where a -20 dB cross-polarization level is observed for the proposed RA antenna no matter what the main beam direction is.

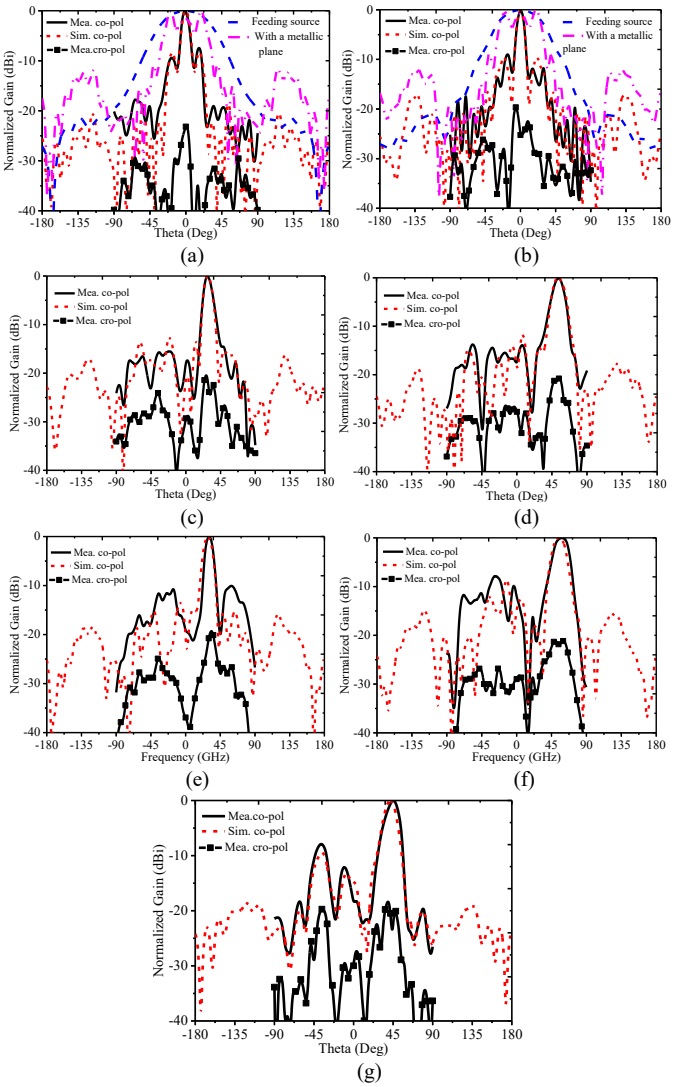

Fig. 13. Measured and simulated normalized realized gains of the proposed RA antenna with different radiation beam directions at 26 GHz. (a). E-plane at broadside. (b). H-plane at broadside. (c). 30 deg off-broadside in E-plane. (d). 60 deg off-broadside in E-plane. (e). 30 deg off-broadside in H-plane. (f). 60 deg off-broadside in H-plane. (g). θ = 45 deg and ϕ = 45 deg.

The radiation performance of the proposed RA antenna is summarized at 26 GHz as listed in Tab. II when its main beam points in a different direction. The simulated total efficiencies are all above 97.0 % at six different main beam directions, which is extremely high. Even though the measured directivities of the proposed RA antenna are not available, it still can be deduced that the total efficiencies of the proposed RA antenna should be high since the measured realized gains considering the heating losses (dielectric, conductor loss) and impedance mismatch of the proposed RA antenna are close to the simulated counterparts very well. Besides, the measured realized gains of the proposed RA antenna at different main beam directions are relatively stable. The measured maximum gain variation of 2.0 dB is observed for the main beam at broadside and 60 deg off-broadside in H-plane.

Tab. II. Radiation performance summary of the proposed RA antenna at 26 GHz.

	Simulated directivity & realized gain	Measured realized gain	Simulated total efficiency	Gain variation in the beam-steerable coverage
θ = 0 deg ϕ = 0 deg	19.6 dBi & 19.5 dBi	18.9 dBi	97.7 %	0 dB
θ = 30 deg ϕ = 0 deg	18.5 dBi & 18.4 dBi	17.9 dBi	97.7 %	1.0 dB
θ = 60 deg ϕ = 0 deg	18.7 dBi & 18.6 dBi	18.2 dBi	97.7 %	0.7 dB
θ = 30 deg ϕ = 90 deg	19.0 dBi & 18.9 dBi	18.3 dBi	97.7 %	0.6 dB
θ = 60 deg ϕ = 90 deg	17.5 dBi & 17.4 dBi	16.9 dBi	97.7 %	2.0 dB
θ = 45 deg ϕ = 45 deg	18.8 dBi & 18.7 dBi	18.3 dBi	97.7 %	0.6 dB

C. Discussion

The proposed RA antenna has some potential application scenarios. First, the proposed RA antenna can provide a fixed beam in any direction, it, therefore, can be served as an antenna with a beam pointing to a prescribed and desired direction. Sometimes, the 2-D beam-steerable capabilities are required but the speed for beam switching is not instant, the proposed RA antenna is a good solution as thoroughly demonstrated in the sections above. For a high-speed beam switching application scenario, the proposed RA antenna is still applicable, where some mini-motors [33] with suitable footprints can be employed to electrically control the rotations of the UCs individually to achieve high-speed manipulations on the main beam directions. The controls of these mini-motors are usually performed by a Field Programmable Gate Array (FPGA) system [20], [21].

We have evaluated the costs of our proposed RA antenna with the previously-reported printed beam-steerable RA antennas by loading PIN diodes. First, the price of metal is relatively cheaper than that of a good quality substrate (Rogers type), and metal is much more available than Rogers type substrates. Second, the price of a PIN diode at the Ka-band is a little expensive than a motor. Most importantly, the PIN diodes seem impossible to be reused again when they are taken off from PCB boards. In contrast, the motors served as control tools can be reused many times. Third, for PIN diodes loaded beam-steerable RA antennas, the configuration of the antenna is multilayer structure (at least two substrate layers) since extra

substrate layers are needed to deploy the DC feeding networks. Sometimes, shorting vias should be drilled within multiple substrate layers for perfect grounding. The multilayer and shorting vias within multiple substrate layers fabrications are all increasing the costs of such antennas. Considering the prices of PIN diodes, substrates, mini-motors, fabrication costs, reuse possibilities, our proposed RA antenna is relatively low-cost and can be produced massively.

V. Conclusion

In summary, a low-cost, high-efficiency and full-metal reflectarray (RA) antenna with mechanically 2-D beam-steerable capabilities is described in this paper. The UC to construct the RA antenna is implemented by a full-metal structure with a cuboid-shaped notch to provide a 1-bit reflection phase for TE and TM normal incidence waves. By adjusting the rotations of UCs manually, the main beam direction of the RA antenna can be easily manipulated on purpose. For demonstration, the main beam at six different directions is presented and measured to validate the concept and effectiveness of the proposed RA antenna for 2-D beam-steerable capabilities. The measured and simulated results on reflection coefficients, radiation patterns, and realized gains are highly consistent. Due to the low-cost, high-efficiency, and high-power handling properties, the proposed RA antenna is a good candidate for 5G millimeter-wave communication applications to provide a fixed or scanning beam.

Acknowledgements

The authors would like to thank the lab engineers, Ben Krøyer and Jesper Dejgaard Meyer for the fruitful discussions on the antenna assembling, Kim Olesen for his kind help with the measurement setup. The author P. Mei would like to thank Mr. P. Liu from the APMS section at Aalborg University for his warm assistance in processing the data. Also, the valuable comments from reviewers and the associate editor are highly appreciated to improve the quality of the manuscript.

References

[1] A. Miura, Y. Fujino, S. Taira, N. Obara, M. Tanaka, T. Ojima, and K. Sakauchi, "S-band active phased array antenna with analog phase shifters using double-balanced mixers for mobile SATCOM vehicles," *IEEE Trans. Antennas Propag*., vol. 53, no. 8, pp. 2533-2541, Aug 2005.

[2] C. Patterson, et al., "A lightweight organic X-band active receiving phased array with integrated SiGe amplifier and phase shifters," *IEEE Trans. Antennas Propag*., vol. 59, no. 1, pp. 100-109, Jan 2011.

[3] M. Abdalla, K. Phang, and G. Eleftheriades, "A planar electronically steerable patch array using tunable PRI/NRI phase shifters," *IEEE Trans, Micro Theory Tech.,* vol. 57, no. 3, pp.531-541, March 2009.

[4] H. Chou, T. Hsiao, and J. Chou, "Active phased array of cavity-backed slot antenna with modified feeding structure for the applications of direction-of-arrival estimation," *IEEE Trans. Antennas Propag*., vol. 66, no. 5, pp. 2667-2672, May 2018.

[5] X. Ding, B. Wang, and G. He, "Research on millimeter-wave phased array with wide-angle scanning performance," *IEEE Trans. Antennas Propag*., vol. 61, no. 10, pp. 5319-5324, Oct 2013.

[6] J. Doane, K. Sertel, and J. Volakis, "A wideband, wide scanning tightly coupled dipole array with integrated balun (TCDA-IB)," *IEEE Trans. Antennas Propag*., vol. 61, no. 9, pp. 4538-4548, Sep 2013.

[7] Y. Cao, L. Chin, W. Che, W. Yang, and E. Li, "A compact 38 GHz multibeam antenna array with multifolded bulter matrix for 5G applications," *IEEE Antennas Wireless Propag. Lett*., vol. 16, pp. 2996-2999, 2017.

[8] W. Yang, Y. Yang, W. Che, C. Fan, and Q. Xue, "94-GHz compact 2-D multibeam LTCC antenna based on multifolded SIW beam-forming network," *IEEE Trans. Antennas Propag*., vol. 65, no. 8, pp. 4328-4333, Aug 2017.

[9] R. Gong, Y. Ban, J. Lian, Y. Liu, and Z. Nie, "Circularly polarized multibeam antenna array of ME dipole fed by 5*6 bulter matrix," *IEEE Antennas Wireless Propag. Lett*., vol. 18, no. 4, pp. 712-717, Apr 2019.

[10] W. Moulder, W. Khalil, and J. Volakis, "60-GHz two-dimensionally scanning array employing wideband planar switched beam network," *IEEE Antennas Wireless Propag. Lett*., vol. 9, pp. 818-821, 2010.

[11] Y. Li, J. Wang, and K. M. Luk, "Millimeter-wave multibeam aperture-coupled magnetoelectric dipole array with planar substrate integrated beamforming network for 5G applications," *IEEE Trans. Antennas Propag.,* vol. 65, no. 12, pp. 6422-6431, Dec. 2017.

[12] I. Mohamed, and A. Sebak, "60 GHz 2-D scanning multibeam cavity-backed patch array fed by compact SIW beamforming," *IEEE Trans. Antennas Propag.,* vol. 67, no. 4, pp. 2320-2331, Apr. 2019.

[13] J. Lian, Y. Ban, Q. Yang, B. Fu, Z. Yu, and L. Sun, "Planar millimeter-wave 2-D beam-scanning multibeam array antenna fed by compact SIW beam-forming network," *IEEE Trans. Antennas Propag.,* vol. 66, no. 3, pp. 1299-1310, March 2018.

[14] H. Kamoda, T. Iwasaki, J. Tsumochi, T. Kuki, and O. Hashimoto, "60-GHz electronically reconfigurable large reflectarray using single-bit phase shifter," *IEEE Trans. Antennas Propag*., vol. 59, no. 7, pp. 2524-2531, July 2011.

[15] H. Yang, F. Yang, S. Xu, Y. Mao, M. Li, X. Cao, and J. Gao, "A 1-bit 10*10 reconfigurable reflectarray antenna: design, optimization, and experiment," *IEEE Trans. Antennas Propag.,* vol. 64, no. 6, pp. 2246-2254, Jun. 2016.

[16] E. Carrasco, M. Barba, and J. Encinar, "X-band reflectarray antenna with switching-beam using PIN diodes and gathered elements," *IEEE Trans. Antennas Propag.,* vol. 64, no. 6, pp. 2246-2254, Jun. 2016.

[17] M. Zhang, et al., "Design of novel reconfigurable reflectarrays with single-bit phase resolution for Ku-band satellite antenna applications," *IEEE Trans. Antennas Propag.,* vol. 64, no. 5, pp. 1634-1641, May. 2016.

[18] H. Zhang, X. Chen, Z. Wang, Y. Ge, and J. Pu, "A 1-bit electronically reconfigurable reflectarray antenna in X-band," *IEEE ACCESS.,* vol. 7, pp.66567-66576, 2019.

[19] T. Debogovic, and J. Perruisseau-Carrier, "Low loss MEMS-reconfigurable 1-bit reflectarray cell with dual-linear polarization," *IEEE Trans. Antennas Propag.,* vol. 62, no. 10, pp. 5055-5060, Oct. 2014.

[20] J. Han, L. Li, G. Liu, Z. Wu, and Y. Shi, "A wideband 1 bit 12 *12 reconfigurable beam-scanning reflectarray: design, fabrication, and measurement," *IEEE Antennas Wireless Propag Letts*, vol. 18, no. 6, pp. 1268-1272, Jun. 2019.

[21] X. Yang, S. Xu, F. Yang, M. Li, Y. Hou, S. Jiang, and L. Liu, "A broadband high-efficiency reconfigurable reflectarray antenna using mechanically rotational elements," *IEEE Trans. Antennas Propag.,* vol. 65, no. 8, pp. 3959-3966, Aug. 2017.

[22] H. Luyen, Z. Yang, M. Gao, J. H. Booske, and N. Behdad, "A wideband, single-layer reflectarray exploiting a polarization rotating unit cell," *IEEE Trans. Antennas Propag.,* vol. 67, no. 2, pp. 872-883, Feb 2019.

[23] H. Luyen, Z. Zhang, J. Booske, and N. Behdad, "Wideband, beam-steerable reflectarrays based on minimum-switch topology, polarization-rotation unit cells," *IEEE ACCESS,* vol. 7, pp. 36568-36578, 2019.

[24] M. Afzal, and K. Esselle, "Steering the beam of medium-to-high gain antennas using near-field phase transformation," *IEEE Trans, Antennas Propag*., vol. 65, no. 4, pp. 1680-1690, Apr 2017.

[25] W. Hong, *et al*., "Multibeam antenna technologies for 5G wireless communications," *IEEE Trans, Antennas Propag*., vol. 65, no. 2, pp. 6231-6249, Dec 2017.

[26] T. Rappaport, *et al*., "Millimeter-wave mobile communications for 5G cellular: it will work," *IEEE ACCESS*, vol. 1, pp. 335-349, 2013.

[27] http://everythingrf.com/products/waveguide-horn-antennas/pasternack-enterprises-inc/617-20-pe9851-2f-10.

[28] P. Mei, S. Zhang, Y. Cai, X. Q. Lin, and G. F. Pedersen, "A reflectarray antenna designed with gain filtering and low-RCS properties," *IEEE*

Trans, Antennas Propag., vol. 67, no. 8, pp. 5362-5371, Aug 2019.
[29] P. Nayeri, M. Liang, R. A. Sabory-Garcia, M. Tuo, F. Yang, H. Xin, and A. Elsherbeni, "3D printed dielectric reflectarrays: low-cost high gain antennas at sub-millimeter waves," *IEEE Trans, Antennas Propag*., vol. 62, no. 4, pp. 2000-2008, Apr 2014.
[30] R. Deng, Y. Mao, S. Xu, and F. Yang, "A single-layer dual-band circularly polarized reflectarray with high aperture efficiency," *IEEE Trans, Antennas Propag*., vol. 63, no. 7, pp. 3317-3320, July 2015.
[31] A. Yu, F. Yang, A. Elsherbeni, J. Huang, and Y. Rahamt-Samii, "Aperture efficiency analysis of reflectarray antennas," *Microw. Opt. Technol Lett*., vol. 52, no. 3, pp. 771-779, Mar. 2004.
[32] H. Yang, F. Yang, S. Xu, M. Li, X. Cao, J. Gao, and Y. Zheng, "A study of phase quantization effects for reconfigurable reflectarray antennas," *IEEE Antennas Wireless Propag Letts*, vol. 16, pp. 302-305, 2017.
[33] https://www.vibrationmotors.com/

Peng Mei (S'15) was born in Suizhou, Hubei province, China, in 1993. He received the B.Sc. and M. Sc. degrees (Hons.) in electromagnetic field and microwave technology from the University of Electronic and Science Technology of China (UESTC), Chengdu, China, in 2015 and 2018, respectively. He is currently pursuing the Ph.D. degree with the Antennas, Propagation and Millimeter-wave Systems section, Department of Electronic Systems, Aalborg University, Aalborg, Denmark.

His current research interests include periodic structures, metasurfaces, millimeter-wave multibeam antennas, and reflectarray/transmitarray antennas,

Mr. Mei was a recipient of the Outstanding Student of UESTC (only ten awardees every year of UESTC) in 2017, the Excellent Graduate Student of UESTC in 2018, the Excellent Graduate Student of Sichuan Province in 2018, and the Excellent Master Thesis from Chinese Institute of Electronics (CIE) in 2019. Mr. Mei was served as a Section Chair in IEEE-APS Topical Conference on Antennas and Propagation in Wireless Communications (APWC), held in Granada, Spain, Sep. 2019.

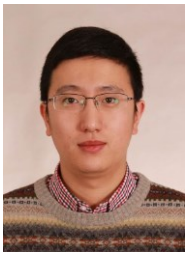

Shuai Zhang (SM'18) received the B.E. degree from the University of Electronic Science and Technology of China (UESTC), Chengdu, China, in 2007 and the Ph.D. degree in electromagnetic engineering from the Royal Institute of Technology (KTH), Stockholm, Sweden, in 2013.

He was a Research Fellow with KTH. In 2014, he joined Aalborg University, Denmark, where he is currently an Associate Professor. In 2010, he joined Lund University, Lund, Sweden, as a Visiting Researcher. In 2011, he joined Sony Mobile Communications AB, Lund, Sweden, as a Visiting Researcher. He was also an external antenna specialist at Bang & Olufsen, Struer, Denmark, from 2016-2017. He has coauthored over 50 articles in well-reputed international journals. He holds more than 16 (US or WO) patents. His current research interests include: mobile terminal mmwave antennas, biological effects, CubeSat antennas, Massive MIMO antenna arrays, UWB wind turbine blade deflection sensing, and RFID antennas.

Gert Frølund Pedersen was born in 1965. He received the B.Sc. and E.E. (Hons.) degrees in electrical engineering from the College of Technology in Dublin, Dublin Institute of Technology, Dublin, Ireland, in 1991, and the M.Sc.E.E. and Ph.D. degrees from Aalborg University, Aalborg, Denmark, in 1993 and 2003, respectively.

Since 1993, he has been with Aalborg University where he is a Full Professor heading the Antennas, Propagation and Millimeter-wave Systems LAB with 25 researchers. He is also the Head of the Doctoral School on wireless communication with some 40 Ph.D. students enrolled. His research interests include radio communication for mobile terminals especially small antennas, diversity systems, propagation, and biological effects. He has published more than 500 peer reviewed papers, 6 books, 12 book chapters and holds over 50 patents. He has also worked as a Consultant for developments of more than 100 antennas for mobile terminals including the first internal antenna for mobile phones in 1994 with lowest SAR, first internal triple-band antenna in 1998 with low SAR and high TRP and TIS, and lately various multiantenna systems rated as the most efficient on the market. He has worked most of the time with joint university and industry projects and have received more than 21 M$ in direct research funding. He is currently the Project Leader of the RANGE project with a total budget of over 8 M$ investigating high performance centimeter/ millimeter-wave antennas for 5G mobile phones. He has been one of the pioneers in establishing over-the-air measurement systems. The measurement technique is now well established for mobile terminals with single antennas and he was chairing the various COST groups with liaison to 3GPP and CTIA for over-the-air test of MIMO terminals. He is currently involved in MIMO OTA measurement.